ELSEVIER

Journal of Alloys and Compounds 388 (2005) 75–82

Journal of ALLOYS AND COMPOUNDS

www.elsevier.com/locate/jallcom

Dissolution of electroless Ni metallization by lead-free solder alloys

Ahmed Sharif, Y.C. Chan*, M.N. Islam, M.J. Rizvi

Department of Electronic Engineering, City University of Hong Kong, Tat Chee Avenue, Kowloon Tong, Hong Kong

Received 14 June 2004; received in revised form 13 July 2004; accepted 13 July 2004

Abstract

An investigation has been carried out to compare the dissolution of the electroless Ni metallization of the ball grid array (BGA) substrate into the molten Sn–0.7 wt.%Cu, Sn–3.5 wt.%Ag–0.5 wt.%Cu and Sn–3.5 wt.%Ag solder. A fixed volume of the BGA solder ball (760 μm diameter) was used on a 4 μm thick electroless Ni(P) metallization over a Cu pad having a circular area with a diameter of 600 μm. The dissolution measurement was carried out by measuring the change of Ni(P) metallization thickness as a function of time and temperature. Scanning electron microscopy was used to examine the microstructure of the solder joint and to measure the consumed thickness of Ni(P). The dissolution in Sn–3.5%Ag solder is higher than in the other two lead-free solders. The presence of Cu in the solder plays a major role in inhibiting the consumption of electroless Ni in the soldering reaction. Despite the fact that the initial formation of intermetallic compounds (IMCs) is the highest in Sn–0.7%Cu solder, the formation of the IMCs and the crystallized Ni_3P is much reduced in the later stage.

Keywords: Lead-free alloys; Electroless Ni; Dissolution; Intermetallic compounds

1. Introduction

Flip chip and ball-grid-array (BGA) technologies are expected to have an increasing share in the microelectronics market in the future [1]. BGA packages offer high input/output pin counts with manageable pitch size and good reliability. The most influential factor in the solder joint quality of a BGA component is the metal surface finish on the Cu pads. Electroless nickel–phosphorus (Ni–P) has attracted much interest and is widely used in the PCB fabrication and under bump metallization (UBM) for flip chip technology. This is because electroless Ni–P offers a low cost alternative to more expensive physical Ni deposition methods. Characteristics of the electroless nickel deposit, such as excellent solderability, corrosion resistance, uniform thickness, and selective deposition, make the electroless nickel plating more suitable as a material for a diffusion barrier than pure electrodeposited Ni UBM [2–4]. However, the electroless Ni is plated by hypophosphite and it is known that the phosphorous (P) in the electroless Ni greatly influences the interfacial reactions with solders [5].

Based on increasing pressures to achieve environmentally friendly electronic materials and processes, and indeed, growing governmental regulations around the world, the drive is strong to use lead-free solders in electronic assemblies [6,7]. This push has highlighted the fact that the industry has not yet arrived at a decision for lead-free solders. The reliability of the lead-free solders has been studied a lot recently, but the knowledge of it is still incomplete and many issues related to them are under heavy debate. The use of new materials will necessitate high standards for reliable, high-density, assembly. Especially a flip chip under bump metallurgy (UBM) comprising few micron thick metal or alloy layers which requires precise designing so that adequate diffusion barriers and good adhesion functions can be fulfilled. At the same time, the UBM layers should not dissolve too strongly into liquid solder bumps and react excessively with them. Since smaller solder volumes are more often encountered in fine and ultra-fine pitch assemblies, it is of great importance to control the metallurgical compatibility of solders with different bump and metallization materials [8]. Since the amount of Ni(P) is limited and some of the Ni(P) must

* Corresponding author. Tel.: +852 27887130; fax: +852 27887579.
E-mail address: eeycchan@cityu.edu.hk (Y.C. Chan).

0925-8388/$ – see front matter © 2004 Elsevier B.V. All rights reserved.
doi:10.1016/j.jallcom.2004.07.015

remain intact through all the reflows and subsequent reworks to avoid the exposure of Cu underneath, the understanding of the consumption rate of Ni(P) is very important. This was a strong motivation for us, to have a closer look at the consumption rate of Ni(P) in the soldering reaction with lead-free solders.

2. Experimental procedure

Electroless Ni(P) layers were deposited on the solder mask defined copper pad of a substrate of the BGA package. The solder mask-opening diameter was 0.6 mm at the ball pad. Special care was taken to make the P content in the deposit as identical as possible. In our case, the P content in the Ni(P) layer is around 10 at.%. An immersion Au plating was immediately layered on top of the electroless Ni–P to avoid oxidation of the nickel surface. The thickness of the deposit layers was measured by using X-ray fluorescence. The thickness of Ni(P) and the immersion Au plating on the surface finish are about 4 μm and 0.5 μm, respectively. Lead-free eutectic Sn–Ag, Sn–Ag–Cu and Sn–Cu solder balls, having the compositions 96.5% Sn–3.5%Ag, 96%Sn–3.5%Ag–0.5% Cu and 99.3% Sn–0.7% Cu (wt.%), respectively, with a diameter of 0.76 mm, were placed on the prefluxed Au/Ni(P)/Cu bond pad of the substrates as shown in Fig. 1 and then soldered isothermally at four different temperatures; 240, 250, 260 and 270 °C for times (t) of 1 (as-reflow), 5, 30, 60 and 120 min in a convection reflow oven. The flux used in this work was a commercial no-clean flux.

To investigate the microstructure, the as-reflowed and extended reflowed samples were mounted with resin, cured at room temperature, mechanically ground and then polished in order to obtain the cross sections of the solder/UBM interfaces. The chemical and microstructural analyses of the gold-coated cross-sectioned samples were obtained by using a Philips XL 40 FEG scanning electron microscope (SEM) equipped with an energy dispersive X-ray spectrometer (EDX). The accuracy of the compositional measurement was about ±3%.

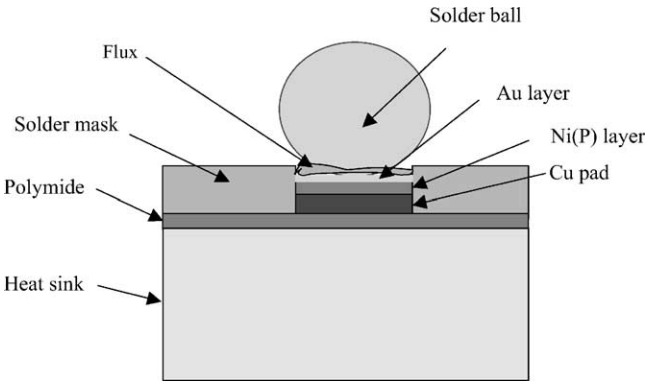

Fig. 1. Solder ball attachment on BGA substrate.

3. Results and discussion

Fig. 2 shows a comparison between different solder alloys of the thickness reduction due to consumption of the

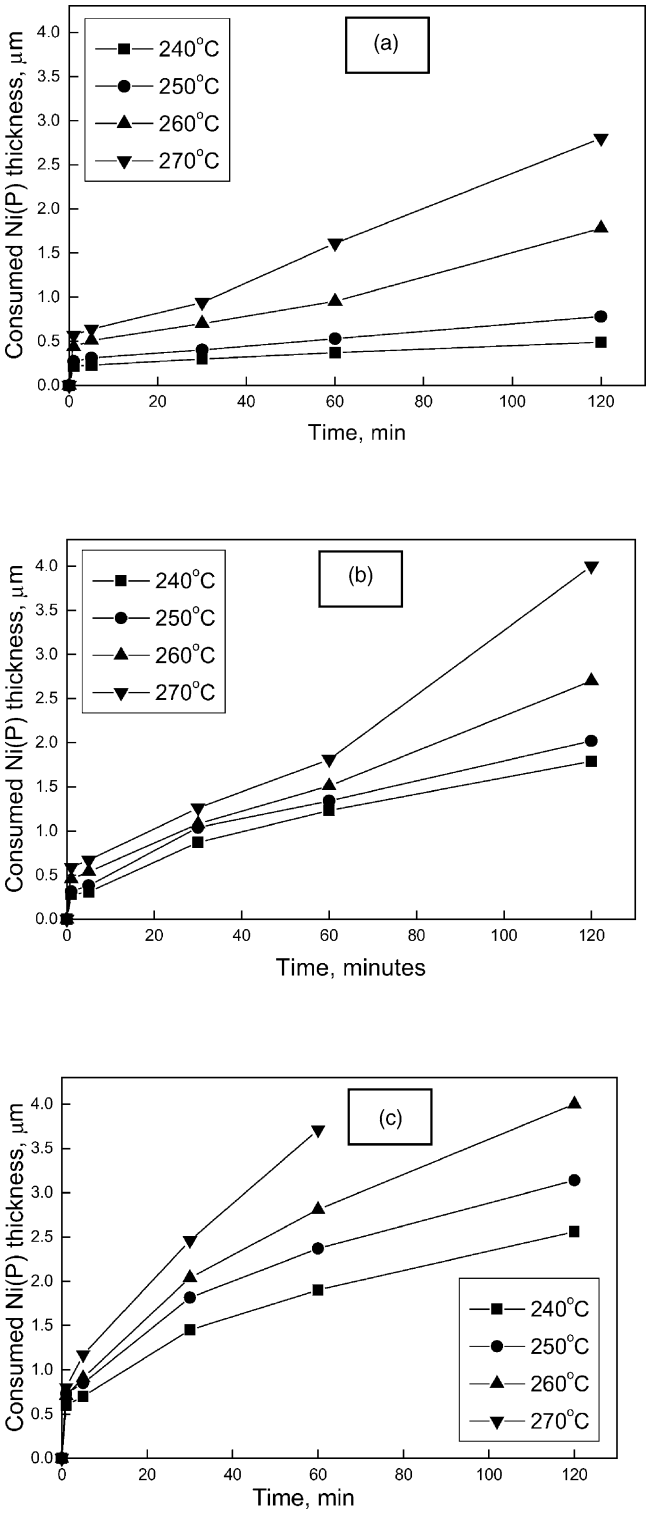

Fig. 2. The consumed thickness of Ni(P) vs. reflow time at four different temperatures for (a) Sn–0.7%Cu, (b) Sn–3.5%Ag–0.5%Cu and (c) Sn–3.5%Ag solder systems.

electroless Ni from the substrate at different temperatures. By measuring the remaining Ni(P) thickness from the SEM micrograph and by subtracting it from the initial thickness, the consumed Ni(P) thickness is deduced. Initial consumption rates are high for all the solder alloys. From this graph, it is also evident that the initial consumption rate is the highest for the highest temperature. It is seen that the consumption of electroless Ni is higher in the Sn–3.5%Ag solder than in the other two Cu-containing solder alloys during extended reflow. Between these latter two Cu-containing solders, Sn–0.7%Cu solder shows less dissolution of the electroless Ni layer than Sn–3.5%Ag–0.5%Cu solder. The melting temperatures of Sn–0.7%Cu, Sn–3.5%Ag and Sn–3.5%Ag–0.5%Cu solder are around 227, 221 and 217 °C, respectively. Thus, the degree of super heating for Sn–3.5%Ag–0.5%Cu solders in the working temperatures is higher than for the other two lead-free solders. However, the dissolution rate in Sn–3.5%Ag–0.5%Cu solder alloy is moderate in each condition in comparison to Sn–3.5%Ag and Sn–0.7%Cu solder.

Fig. 3 shows the microstructures of the as-reflowed interface between the Au/Ni(P)/Cu bond pad and the Pb-free solders at 250 °C. Cu-containing solders exhibit higher intermetallic compounds (IMCs) thickness than Sn–3.5%Ag solder. Between the two Cu-containing solders, the IMCs thickness is higher in Sn–0.7%Cu solder interface after as-reflowed. According to EDX analysis, the IMCs in the Cu-containing solders is composed of Cu–Ni–Sn i.e. $(Cu_{1-x}Ni_x)_6Sn_5$ and is based on Cu_6Sn_5. The atomic percentage of Cu in the Cu–Ni–Sn ternary IMCs is higher in the Sn–0.7%Cu solder than in the Sn–0.7%Cu solder. It can be concluded that Cu–Ni–Sn ternary IMCs with a high amount of Cu grows faster in the initial state of reflow. On the other hand, Ni_3Sn_4-based binary IMCs form in the Sn–3.5%Ag solder interface. It is already known that Cu_6Sn_5 binary IMC grows as a large scallop-type grains projected toward the solder [8,9]. From Fig. 3 it can be also seen for Sn–0.7%Cu solder that Cu–Ni–Sn ternary IMCs with more Cu show a similar scallop-type growth.

The avarage thickness of intermetallic compounds at the solder–substrate metallization interface after reflow at various temperatures for different durations are shown in Fig. 4. The initial growth rate of the IMCs is high for all the solder systems. It is also evident that the Cu–Ni–Sn IMCs in the Cu-containing solder systems grow much faster than the Ni–Sn IMCs in the Sn–3.5%Ag system during extended reflow. It is well-known that reaction kinetics of the Cu_6Sn_5-based compound is faster than those of the Ni_3Sn_4-based compound [8–11]. In the case of Sn–3.5%Ag solder, the IMC is always Ni_3Sn_4. A sudden increase in the growth of IMCs for Sn–3.5%Ag solder is observed after 60 min reflow at 260 and 270 °C (Fig. 4c). This sudden increase is related to the dissolution of the whole electroless Ni metallization and as well as the Cu pad. The percentage of Cu in the interfacial ternary Cu–Ni–Sn IMCs is higher in the Sn–0.7%Cu solder than in the Sn–3.5%Ag–0.5%Cu solder for all the conditions. During long time molten reaction, bright low-Cu ternary IMCs appears earlier at the interface of the Sn–3.5%Ag–0.5%Cu solder than the Sn–0.7%Cu solder (Fig. 5a and b). Due to

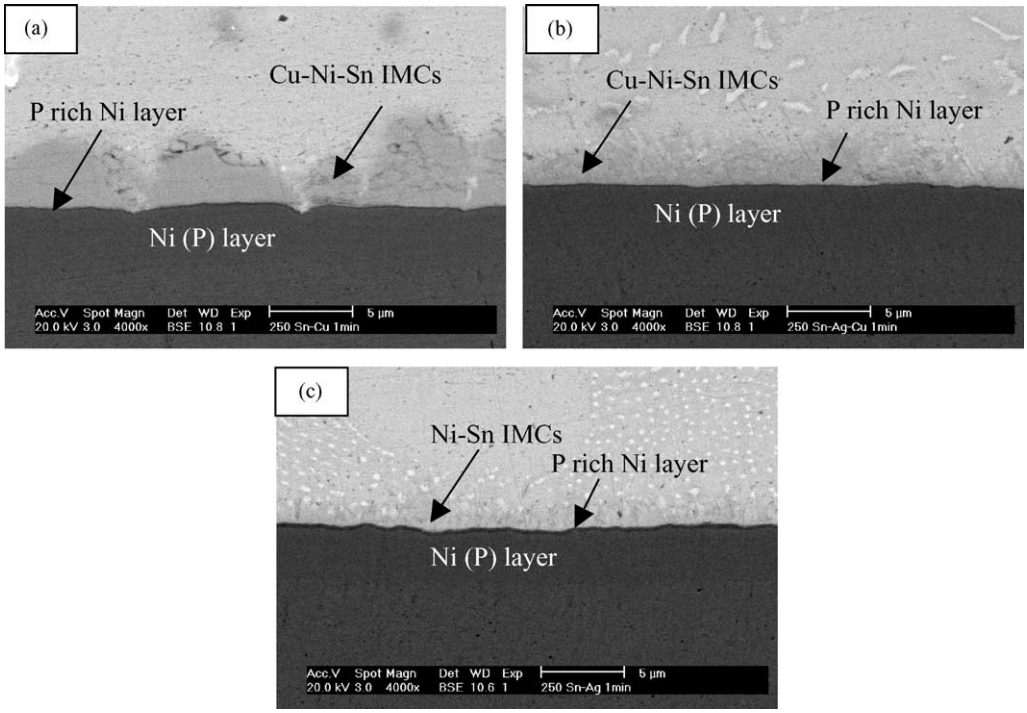

Fig. 3. Backscattered electron micrographs illustrating the interface after reflowed at 250 °C of (a) Sn–0.7%Cu, (b) Sn–3.5%Ag–0.5%Cu and (c) Sn–3.5%Ag solders.

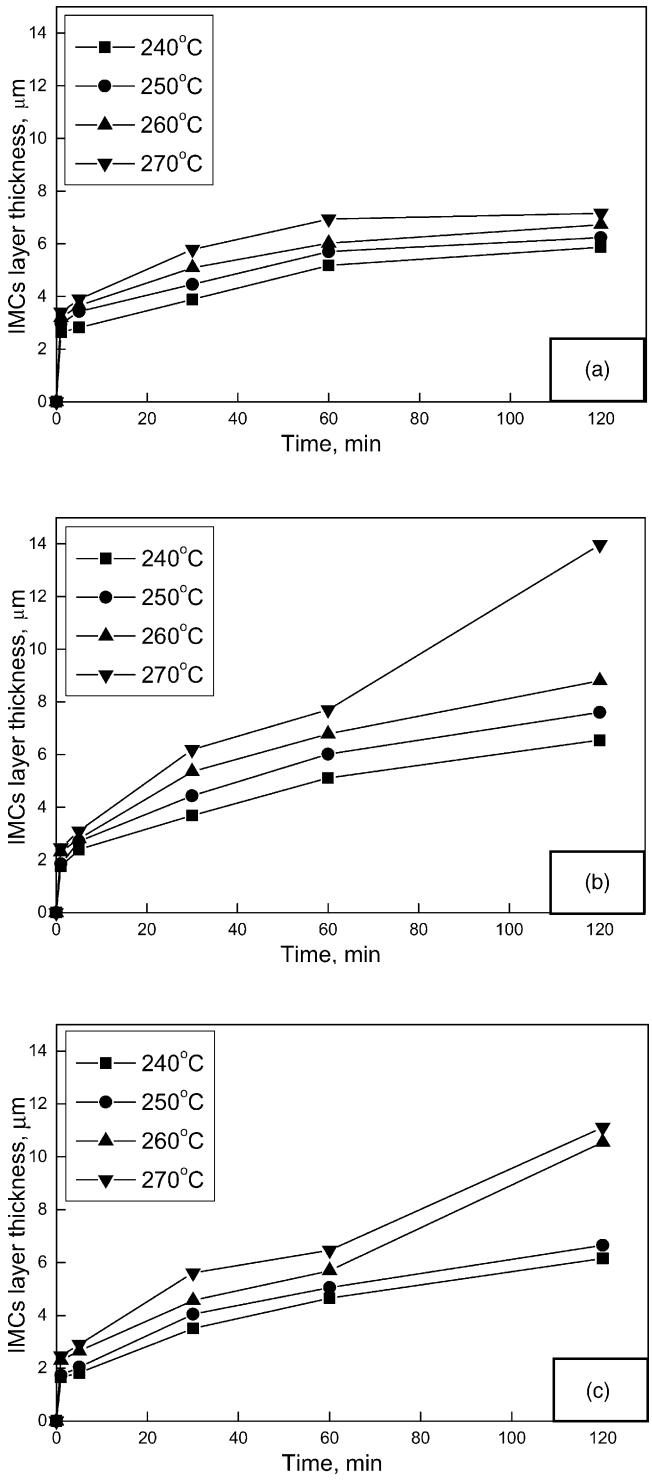

Fig. 4. Growth of intermetallic compound layers in (a) Sn–0.7%Cu, (b) Sn–3.5%Ag–0.5%Cu and (c) Sn–3.5%Ag solder systems at four different temperatures.

the long time molten reaction, these bright IMCs grow beneath the relatively dark high-Cu Cu–Ni–Sn IMCs layer, as most of the Cu in the bulk solder has been consumed and is incorporated in the upper ternary IMCs.

Fig. 6 illustrates the backscattered electron micrographs of the interface after reflow for 2 h at 270 °C. In Sn–3.5%Ag solder, high dissolution of the surface metallization as well as the Cu pad is observed. As soon as the original Ni(P) layer is consumed, the molten solder reacts rapidly with the Cu pad. It is already proven that the dissolution rate of Cu in Sn–3.5%Ag solder is very high [12]. Another important fact to be noted is that with extended reflow the dark Ni_3P layer also becomes exhausted and a trace of white Sn–Ni–P is observed at the position of the dark Ni_3P layer (Fig. 6c). Through EDX analysis some P is also detected in the Ni–Sn IMCs. For Sn–3.5%Ag–0.5%Cu solder, the original Ni(P) layer is nearly consumed in most places of the interface. At this stage, a layer type spalling is observed (Fig. 6b). It may be stated that when the supply of Ni from the pad is ended, spalling starts to occur at the interface of the Sn–3.5%Ag–0.5%Cu/Ni(P) system. A thick white layer forms over the Ni_3P layer at the expense of Ni_3P layer. In those specific areas, the Sn rich molten solder comes in direct contact with the Ni_3P layer and reacts to form Ni–Sn–P compound. Below the Ni_3P layer, another bright layer is also detected at this stage. This layer is determined to be Cu_3Sn phase through EDX. The existing Ni_3P layer limits the supply of Sn from the solder more than Cu from the substrate, so Cu_3Sn forms beneath the Ni_3P layer. In the Sn–0.7%Cu system a layer type spalling is observed (Fig. 6a). Still some of the IMCs are well attached to the substrate with the original Ni(P) even after 2 h of reflow at 270 °C. Another important fact to be noticed is that no Au resettlement is observed for any of the solder system under such high temperature molten condition.

In the extended molten reaction, the IMCs start to break and spall of from the interface. Spalling is more severe at higher temperatures. More spalling is observed in Sn–0.7%Cu solder. So it may be stated that Cu rich IMCs are more prone to spalling. There is also a high increase in the consumption of Ni(P) observed at 260 and 270 °C after long time molten condition for the Sn–Cu solder (Fig. 2a). This increase in consumption of Ni(P) may also be related to the high spalling of the IMCs from the interface. Even at low temperature, in few places of the interface in Sn–0.7%Cu solder after severe spalling, the diffusion path of the reacting species is reduced thus more reaction takes place at the interface. In that case, a high consumption of electroless Ni with the formation of a thick P rich Ni layer is observed at the interface (Fig. 7a). No spalling is noticed even at 270 °C in Sn–3.5%Ag solder.

For all the solder alloys the thickness of the P rich Ni layer also increases with reflow, but for Sn–3.5%Ag solder the rate is the highest. For Sn–0.7%Cu solder, the thickness of the P rich Ni layer does not increase too much even at 270 °C for extended period of reflow. Beyond 60 min reflow at 260 and 270 °C, the thickness of the Ni_3P layer does not increase in Sn–3.5%Ag solder system and some channels are observed in the Ni_3P layer. It is important to note that the growth of Ni_3P in Sn–3.5%Ag is higher than that in the other two solder alloys whereas IMCs growth is relatively less.

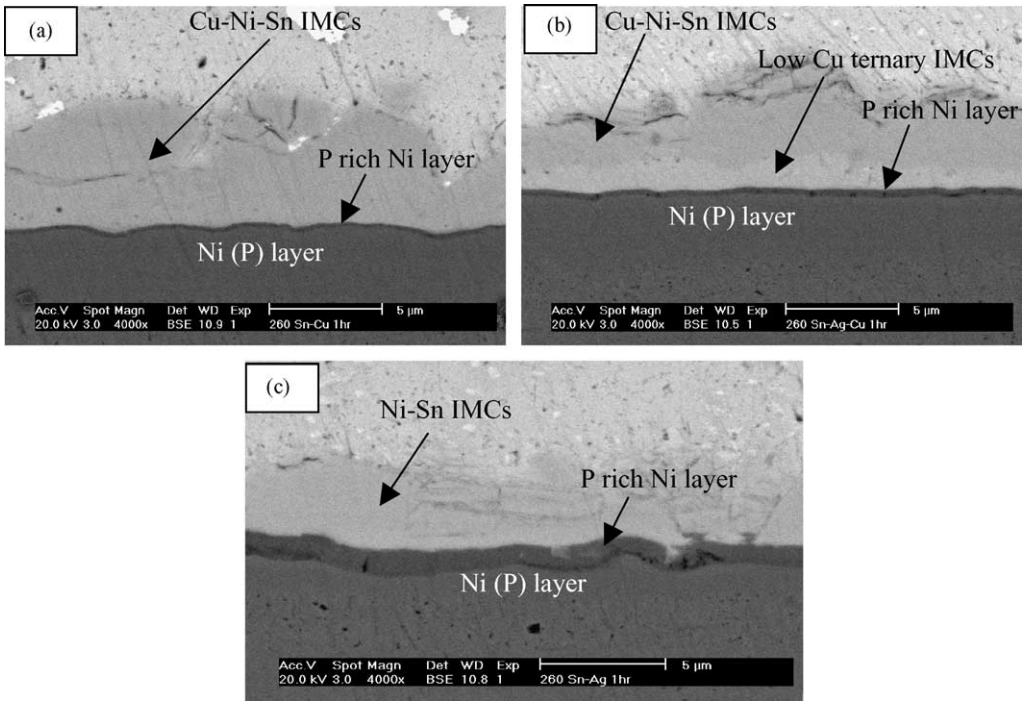

Fig. 5. SEM micrographs showing the interface after reflowed for 1 h at 260 °C of (a) Sn–0.7%Cu, (b) Sn–3.5%Ag–0.5%Cu and (c) Sn–3.5%Ag solders.

So the consumption of electroless Ni in Sn–3.5% Ag is also attributed to the high growth rate of the P rich Ni layer.

Fig. 8(i) shows plots of the Ni_3P thickness^2 versus time at various temperatures. Each plot displays a linear relationship, so it can be assumed that the growth of Ni_3P in the lead-free solders is controlled by a diffusion process. The formation of Ni_3P in Pb–Sn solder is also proven to be diffusion controlled [13]. The growth kinetics of Ni_3P is studied using the rate equation $K = K_o\exp(-Q/RT)$, where Q is the activation energy for interdiffusion of Ni and P and K_o is the the rate constant. The slope of the lines representing plots of the square of the Ni_3P thickness versus time, gives the rate constant, K. The Arrhenius plot of the natural logarithm of K versus $1/T$, as shown in Fig. 8(ii), gives the activation energy for diffusion. From this plot, E is found to be 131, 103 and 75 kJ/mol for Sn–0.7%Cu, Sn–3.5%Ag–0.5%Cu and Sn–3.5%Ag, respectively for the above condition and K_o is estimated to be 3.39×10^{-4} m^2/s, 2.84×10^{-6} m^2/s and 1.1×10^{-8} m^2/s. The highest activation energy found in Sn–0.7%Cu solder implies that the formation of the P-rich crystallized Ni–P compound should be more difficult than in the other two lead-free solders.

In ternary Cu–Ni–Sn IMCs, around 20 at.% of Ni is present, whereas in binary Ni–Sn IMCs, the atomic percentage of Ni is around 43. Thus, the consumption of Ni from the substrate to produce a 1 μm thick IMCs layer is twice as large in the Sn–3.5%Ag solder interface than in the Cu-containing solder. Though the thickness of the IMCs in the Sn–3.5%Ag solder is relatively less, the overall consumption of Ni is much higher. In case of Sn–0.7%Cu solder, the ternary IMCs contain more Cu and less Ni. So the formation of Cu rich ternary IMCs in Sn–0.7%Cu solder consumes less Ni. Another point is that in case of Sn–3.5%Ag–0.5%Cu, the bright low-Cu ternary appears earlier and the structure of these IMCs is based on Ni_3Sn_4. More Ni is consumed during the formation of such low-Cu ternary IMCs. Thus the overall consumption of electroless Ni is relatively higher in Sn–3.5%Ag–0.5%Cu solder than in Sn–0.7%Cu solder. It is already noticed that the consumption of the original Ni(P) layer in the Sn–3.5%Ag solder is the highest. Due to the consumption of Ni to form interfacial IMCs, P is expelled to the remaining Ni–P layer and forms a P-rich Ni layer. It is realistic to anticipate that the higher the interfacial reaction, the greater is the tendency to form a continuous P-rich Ni layer. According to the EDX analysis, the P content in the original Ni(P), which is about 10 at.% before soldering, decreases to around 8.1 at.% from the top of the original Ni(P) layer after reflow. It can be stated that the Ni_3P crystallization is a simultaneous process along with IMCs fromation. It means that Ni_3P formation does not only depend on the P accumulation during the Ni consumption due to IMCs formation.

Rapid diffusion of one material into another can cause crystal vacancies to form in the bulk material. These vacancies attract each other which results in the creation of voids. These voids are called Kirkendall voids [14]. For long time reflow, a high amount of Kirkendall voids may be generated at the Ni_3P layer during the diffusion process and some channels may also be created by the coalescence of these Kirkendall voids [15]. Due to this, a high dissolution of the electroless Ni layer is observed in those specific places. Through these

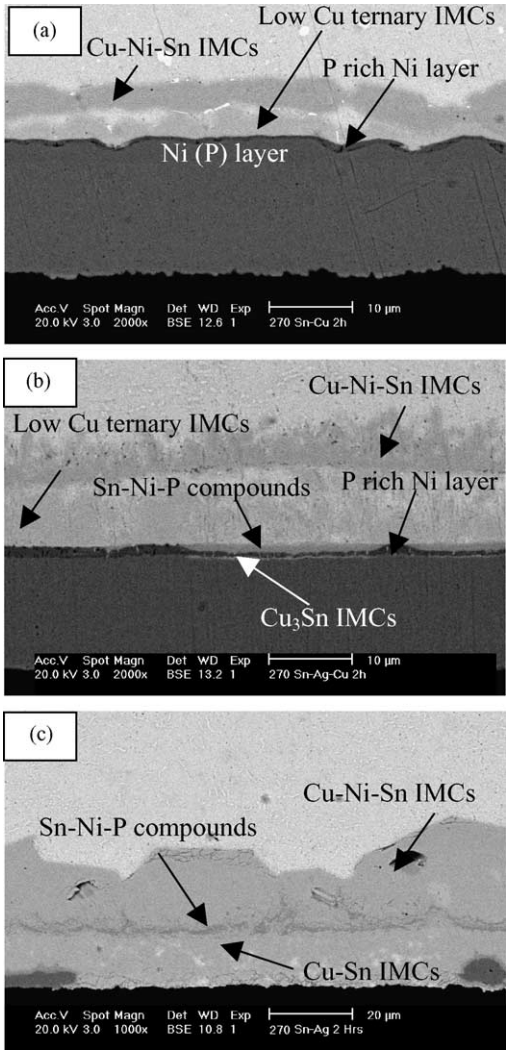

Fig. 6. SEM micrographs showing the interface after soldering for 2 h at 270 °C of (a) Sn–0.7%Cu, (b) Sn–3.5%Ag–0.5%Cu and (c) Sn–3.5%Ag solders.

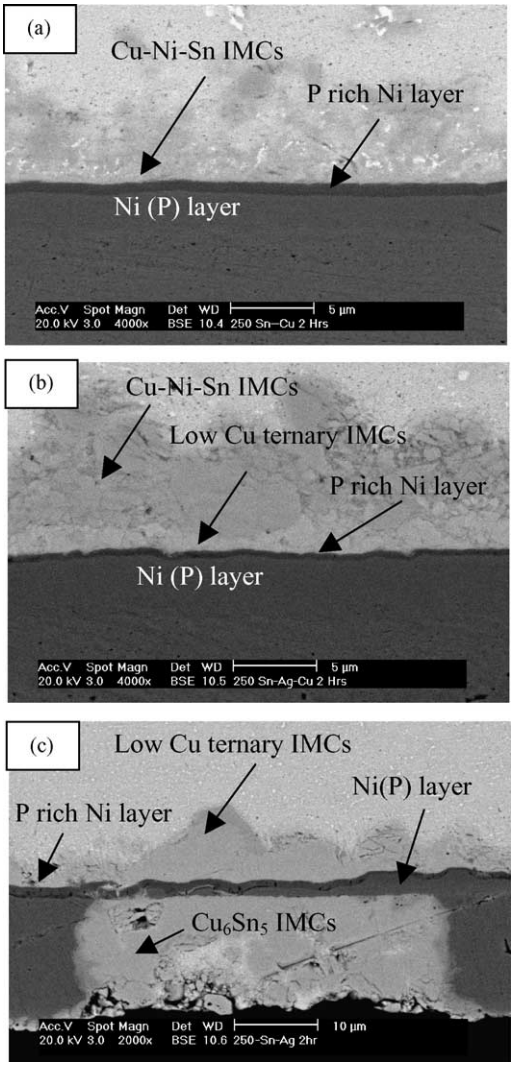

Fig. 7. SEM micrographs showing the interface after reflowed for 2 h at 250 °C of (a) Sn–0.7%Cu, (b) Sn–3.5%Ag–0.5%Cu and (c) Sn–3.5%Ag solders.

channels, molten metal comes into contact with the Cu layer underneath the electroless Ni layer. Thus even at low temperatures, a high dissolution of the Cu layer is observed with the presence of the original Ni(P) at most of the places along the interface (Fig. 7c).

As the IMCs at the interface is plainly Ni_3Sn_4 in the Sn–3.5%Ag solder system, a simplistic theoretical approach can be used to determine the IMCs thickness at the interface of the solder by measurement of the Ni(P) consumption from the substrate and the thickness of the P rich Ni layer. The solder balls have a volume of $2.29 \times 10^{-4}\,\mathrm{cm}^3$. As the solubility of Ni in Sn is very low, assuming that the total consumption of Ni from the substrate is equal to the Ni in the interfacial intermetallic compounds and the dark Ni_3P layer at the interface, from the mass balance of Ni,

$$f_{\mathrm{Ni(P)}}\Delta h_{\mathrm{Ni(P)}}A\rho_{\mathrm{Ni(P)}} = f_{\mathrm{Ni(D)}}\Delta h_{\mathrm{D}}A\rho_{\mathrm{D}} + f_{\mathrm{Ni(C)}}\Delta h_{\mathrm{C}}A\rho_{\mathrm{C}}$$

where $\Delta h_{\mathrm{Ni(P)}}$ is the consumed thickness of Ni(P); Δh_{D} and Δh_{C} are the thickness of the dark Ni_3P layer and interfacial intermetallics, respectively; A is the total interfacial area between solder and Ni; $\rho_{\mathrm{Ni(P)}}$, ρ_{D} and ρ_{C} are the density of the Ni(P) layer, dark Ni_3P layer and interfacial intermetallics, respectively and f is the weight fraction of Ni in the respective layer. From the experimental measurement, one obtains a value for the total interfacial area, $A = 2.83 \times 10^{-3}\,\mathrm{cm}^2$ and which will be used in conjunction with the values of the material constants $\rho_{\mathrm{Ni(P)}} = 8.527\mathrm{g/cm}^3$, $\rho_{\mathrm{D}} = 7.823\,\mathrm{g/cm}^3$ and $\rho_{\mathrm{C(Ni–Sn)}} = 8.642\,\mathrm{g/cm}^3$ [13]. Fig. 9 shows the thickness of the Ni_3Sn_4 compounds as a function of time at 250 °C for Sn–3.5%Ag solder. The solid line and the square symbols show the measured and calculated thickness of the Ni_3Sn_4 compounds, respectively. The good agreement between the solid line and the squares indicates that the soldering reaction in the Sn–3.5%Ag/Ni(P) system is conservative and Ni does not dissolve in to the solder but remains at the interface.

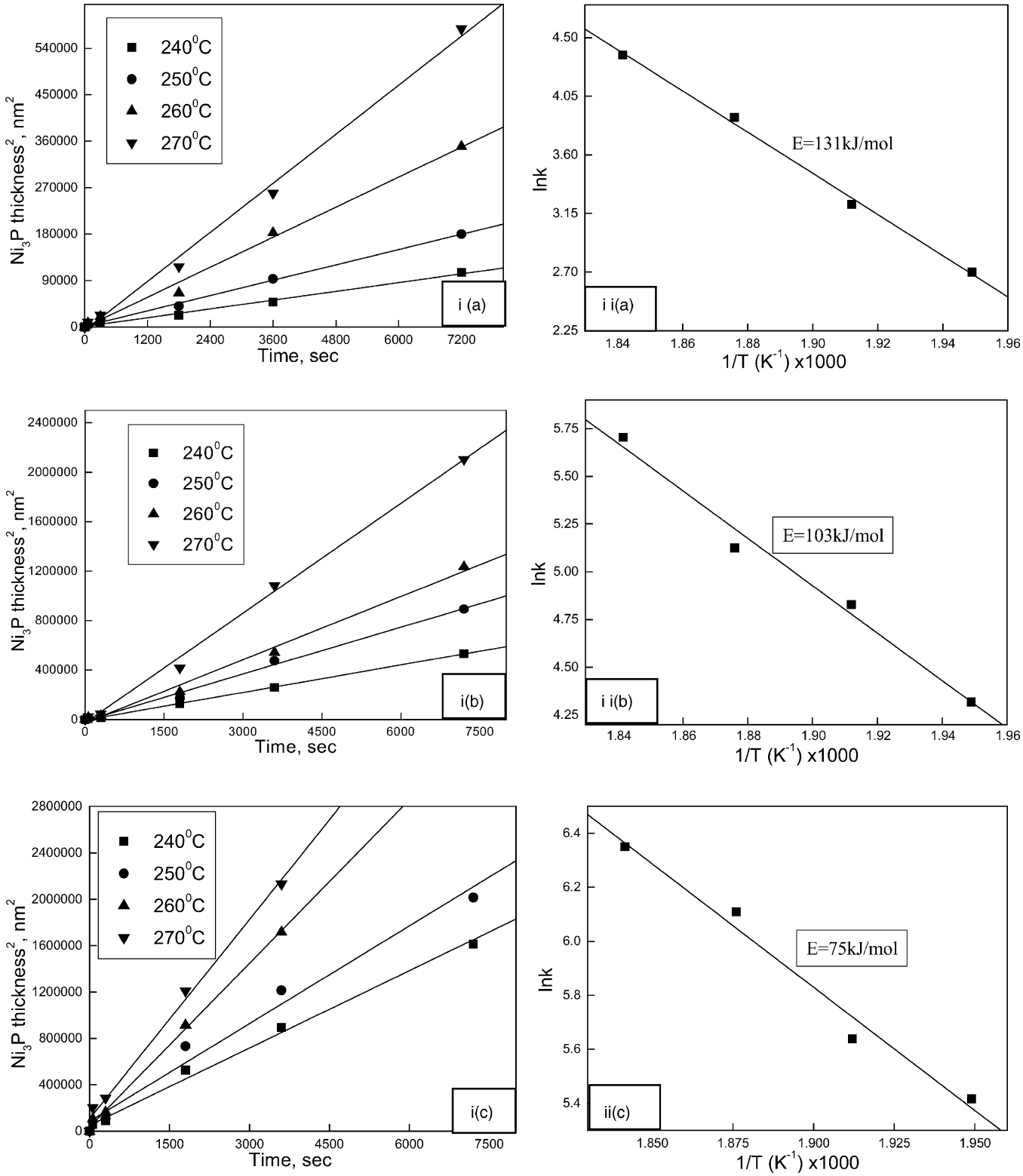

Fig. 8. (i) Ni_3P layer thickness squared vs. time at various temperatures and (ii) Arrhenius plot of diffusivity vs. $1/T$ to determine the activation energy of (a) Sn–0.7%Cu, (b) Sn–3.5%Ag–0.5%Cu and (c) Sn–3.5%Ag solders.

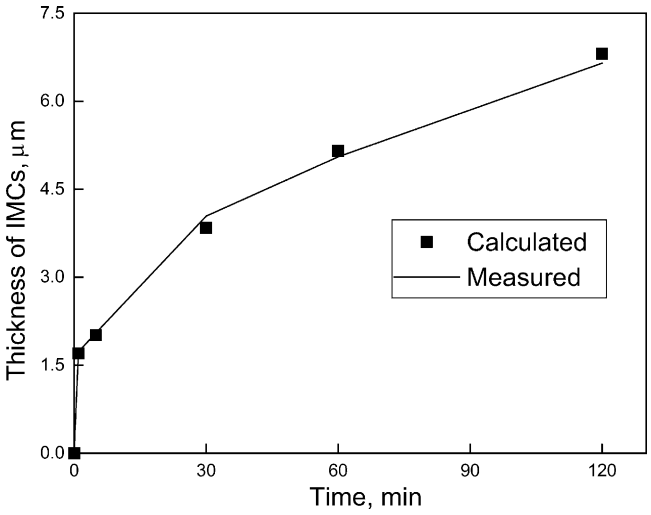

Fig. 9. Thickness of Ni_3Sn_4 compounds as a function of time at 250 °C for Sn–3.5%Ag solder. The solid lines and square symbols show the measured and calculated thickness of Ni_3Sn_4 compounds, respectively.

4. Conclusions

The effect of reflow at four different temperatures (240, 250, 260 and 270 °C) on the dissolution of Ni(P) surface finish in Sn–3.5%Ag, Sn–3.5%Ag–0.5%Cu and Sn–0.7%Cu BGA solder balls are presented in this paper. A very fast dissolution of the substrate is observed in the early stage of the molten solder/solid Ni(P) reaction for all the solder alloys. Cu-containing lead-free solders exhibit less dissolution of electroless Ni during the long time reflow condition. The diffusion of reacting species through the more Cu-containing ternary IMCs is restricted in the extended period of molten reaction. Sn–0.7%Cu solder demonstrates formation of much IMCs in the initial stage. However, the formation of IMCs and crystallized Ni_3P in Sn–Cu solder is reduced under the long reflow condition. It is also seen that the formation of Ni_3P on electroless Ni(P) with lead-free solders is diffusion controlled. From the theoretical approach, it is found that though the dissolution of the electroless Ni is the highest, the soldering reaction is conservative and Ni does not dissolve in to the bulk solder in Sn–3.5%Ag solder.

Acknowledgements

The authors would like to acknowledge the financial support provided by Research Grant Council of Hong Kong for the project “Wetting Kinetics and Interfacial Interaction Behavior between Lead-free Solders and Electroless Nickel Metallizations,” CERG project no. CityU 1187/01E (CityU ref. 9040621) and the research studentship of City University of Hong Kong.

References

[1] “International Technology Roadmap for Semiconductor” Semiconductor Industry Association, San Jose, CA, USA, 1999.
[2] T. Komiyama, Y. Chonan, J. Onuki, T. Ohta, Mater. Trans. 43 (2002) 227–231.
[3] K.C. Hung, Y.C. Chan, C.W. Tang, H.C. Ong, J. Mater. Res. 15 (2000) 2534–2539.
[4] M. Inaba, K. Yamakawa, N. Iwase, IEEE Trans. CHMT 13 (1990) 119–123.
[5] Y. Jeon, K. Paik, in: Proceeding of the 51st Electronic Components and Technology Conference, 2001, pp. 1326–1331.
[6] K. Zeng, K.N. Tu, Mater. Sci. Eng. Rep. 38 (2002) 55–105.
[7] M. Abtew, G. Selvaduray, Mater. Sci. Eng. Rep. 27 (2000) 95–141.
[8] K. Kulojärvi, V. Vuorinen, J. Kivilahti, Microelectron. Int. 15 (1998) 20–24.
[9] T.M. Korhonen, P. Su, S.J. Hong, M.A. Korhonen, Y.C. Li, J. Electron. Mater. 29 (2000) 1194–1199.
[10] P.G. Kim, J.W. Jang, T.Y. Lee, K.N. Tu, J. Appl. Phys. 86 (1999) 6746–6751.
[11] S. Barder, W. Gust, H. Hieber, Acta Metall. Mater. 43 (1995) 329–337.
[12] A. Sharif, Y.C. Chan, Mater. Sci. Eng. B 106 (2004) 126–131.
[13] J.W. Jang, P.G. Kim, K.N. Tu, D.R. Frear, P. Thompson, J. Appl. Phys. 85 (1999) 8456–8462.
[14] NASA Goddard Space Flight Center, Wire Bond Website, http://nepp.nasa.gov/wirebond/intermetallic_creation_and_growt.htm.
[15] M.N. Islam, Y.C. Chan, A. Sharif, M.O. Alam, J. Microelectron. Reliability 43 (2003) 2031–2037.